Paschen's curve in microgaps with an electrode surface protrusion

Yangyang Fu,[1,2,a)] Peng Zhang,[2] and John P. Verboncoeur[1,2]
[1]*Department of Computational Mathematics, Science and Engineering, Michigan State University, East Lansing, Michigan 48824, USA*
[2]*Department of Electrical and Computer Engineering, Michigan State University, East Lansing, Michigan 48824, USA*

(Received 18 June 2018; accepted 4 July 2018; published online 3 August 2018)

Paschen's curve in microgaps with a hemi-ellipsoidal protrusion on the electrode surface is studied using a two-dimensional fluid model. The breakdown voltage is identified when the discharge enters the subnormal region, according to voltage-current characteristics. It is found that the breakdown in a microgap with a surface protrusion on the electrode can result in a combined Paschen's curve, which transits from long-gap (distance between the cathode and anode without the presence of protrusion) behavior at low pressure to short-gap (distance between the protrusion apex to the opposite electrode) behavior at high pressure. As gas pressure decreases, the length of the optimal discharge path increases, automatically moving from the top of the protrusion to its side surface and then to the wider non-protrusion electrode gap. The effects of the protrusion height and radius as well as the discharge polarity on the Paschen's curve are examined in detail. The effects of the protrusion aspect ratio on field enhancement are also considered. This work provides insights into the design of microgaps with controlled breakdown voltage across many orders in pressure via engineered electrode morphology. *Published by AIP Publishing.* https://doi.org/10.1063/1.5045182

Gas breakdown in microplasmas and microdischarges with characteristic lengths less than 1 mm is key in many applications, including micro-electro-mechanical systems (MEMS), micro-switches, and microchip devices.[1–3] Paschen's curve, which describes the breakdown voltage as a function of the combined parameter pd (gas pressure $p \times$ gap distance d), under an often assumed uniform electric field, is an effective way to analyze the electrical characteristics of the macroscale gas gap.[4–8] In recent years, 3D printing technology enables increasingly complicated geometries in plasma devices down to the micron scale.[9,10] Previous studies show that the discharge properties can be largely affected by the electrode geometry or surface roughness.[11–13] Controlling the electrode geometry in microgaps might be one effective way to control the system variability such as the voltage hold-off. Recent advances in diagnostics and modeling of complex plasma systems opened an opportunity to identify new characteristics of the gas breakdown in microgaps under direct-current (DC) fields and also other discharges.[14,15] A DC microgap breakdown at atmospheric pressure is ignited and maintained by secondary electron emission when the gap distance is greater than $\sim 10\,\mu$m, whereas field emission becomes dominant when the gap distance is less than a few microns, especially with microprotrusions on the cathode surface.[16–18] It was found that the Townsend scaling law still holds for discharges in microgaps unless the field emission becomes dominant.[19–21]

Characterizing a parallel-plane microdischarge at high pressure is not easy since discharge instabilities often occur, especially with the presence of the protrusion on the electrode surface. This surface protrusion usually leads to the enhancement of the local electric field. The field enhancement may not necessarily bring the discharge into the field emission regime unless the electric field reaches the order of 10^9 V/m.[22] For normal atmospheric discharges with hundreds of microns gap length, the electric field is usually in the order of 10^7 V/m and the discharge is still mainly sustained by the ion-impact secondary electron emission on the cathode.[23] A series of investigations of the modified Paschen's curve combining the secondary electron emission and the field emission were carried out in Refs. 23–28. However, even without the field emission, the protrusion will change the gap geometry and thus impact the electric field distributions and the charge fluxes,[12,13] which may significantly change the shape of breakdown curves.

This work focuses on the impact of the electrode surface protrusion on Paschen's curves in microgaps. Using a two-dimensional fluid model, the Townsend breakdown voltages in microgaps are quantified based on the voltage-current characteristics when the discharge enters the subnormal region with a negative differential resistance. The effects of the protrusion parameters, such as the protrusion height and radius, as well as the discharge polarity, on the Paschen's curves in microgaps are examined.

The schematic of the microgap is shown in Fig. 1. A DC voltage U_{dc} is applied to the anode through a ballast resistor $R_b = 100\,\text{k}\Omega$, while the cathode is grounded. The microgap consists of two plane-parallel circular electrodes with a single hemi-ellipsoidal protrusion on the cathode. The electrode protrusion results in the minimum distance, d_{min}, from the tip to the opposite anode. The maximum gap distance, d_{max}, is between the flat surface of the cathode and the anode. The coordinates are in the r–z plane, and R is the electrode radius. In all cases, $d_{max} = 500\,\mu$m and $R = 1000\,\mu$m, and the impact of the aspect ratio of the microgap (related to the transverse diffusion) can be excluded since the sidewall is relatively far

[a)]Author to whom correspondence should be addressed: fuyangya@egr.msu.edu

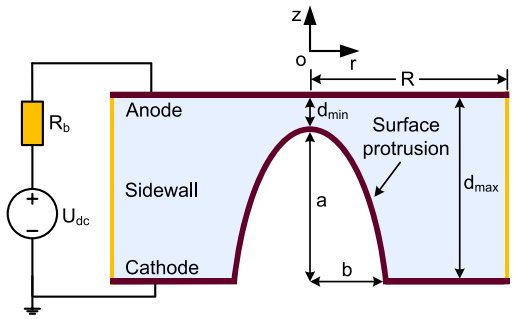

FIG. 1. A DC voltage source applied to a microgap with a hemi-ellipsoidal protrusion on the cathode surface through a ballast resistor.

from the axis.[13] The geometry of the protrusion is characterized by the protrusion height a and the radius b. Argon gas at room temperature 300 K (0.026 eV) is chosen as the working gas. In the cases studied, the discharge is sustained by ion-impact secondary electron emission at the cathode, where field emission can be ignored since the shortest distance d_{min} is no less than 50 μm and the maximum effective electric field including the modest field enhancement of the hemi-ellipsoidal tip is much smaller than 10^9 V/m.[16–18] The normal flux of electrons emitted by the cathode is related to the flux of incident ions by an effective secondary emission coefficient γ, which is fixed at 0.1.[29,30] The equations of the model are solved self-consistently to reach steady-state, and the detailed description of the fluid model can be found in previous studies.[31–34]

Figure 2 shows the calculated breakdown voltage as a function of gas pressure for a microgap with a hemi-ellipsoidal protrusion ($a = 450\ \mu$m and $b = 200\ \mu$m) on the cathode surface, resulting in $d_{min} = 50\ \mu$m and $d_{max} = 500\ \mu$m (see Fig. 1). It can be seen that the Paschen's curve shifts from the low-pressure regime for the long gap ($d = 500\ \mu$m) to the high-pressure regime for the short gap ($d = 50\ \mu$m). The lowest point of the Paschen's curve for parallel plate gaps (without protrusion) of $d = 50\ \mu$m and $d = 500\ \mu$m is about 1.0–1.5 Torr cm, which is close to the Paschen's minimum (Stoletov point) for argon.[35,36] Although a more accurate description of the discharge may require the kinetic treatment of electrons, the

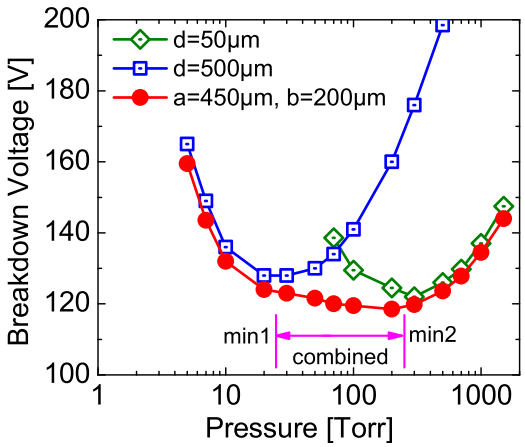

FIG. 2. The calculated breakdown voltage as a function of gas pressure for a cathode hemi-ellipsoidal protrusion ($a = 450\ \mu$m and $b = 200\ \mu$m) compared to the parallel-plate gap with $d = 50\ \mu$m and $d = 500\ \mu$m spanning the maximum and minimum for the protrusion case.

current model is employed to understand the qualitative trends of the breakdown curves with the perturbation of the protrusion geometry.[37,38] The cathode surface protrusion results in a combined Paschen's curve, which transits from long-gap behavior at low pressure to short-gap behavior at high pressure, resulting in relatively low breakdown voltages in a wider range of pressures. This is due to the migration of the major discharge path as the pressure changes, which will be explained below.

The discharge channels represented by the ion density near the cathode are shown in Fig. 3 with $U_{dc} = 150$ V. The gas pressures in Figs. 3(a)–3(d) are 500 Torr, 100 Torr, 50 Torr, and 10 Torr, respectively. At the high pressure, as shown in Fig. 3(a), the discharge mainly occurs between the protrusion tip and the opposite anode, which is the shortest discharge path. As the pressure decreases, as shown in Figs. 3(b) and 3(c), the discharge follows a longer path and the cathode emission migrates along the protrusion surface. When the pressure is much lower, as shown in Fig. 3(d), the discharge mainly occurs between the anode and the cathode substrate.

The self-adjusted discharge paths at different pressures can be explained based on the mean free path of electron-neutral collision. According to Paschen's law, the Stoletov point with the lowest breakdown voltage is

$$(pd)_{\text{Stoletov}} = \frac{\exp(1) \cdot \ln(1/\gamma)}{A}, \tag{1}$$

where the constant $A = \sigma_{en}/(k_B T_g)$, σ_{en} is the electron-neutral collision cross section, k_B is Boltzmann's constant, and T_g is the temperature of the neutral gas.[35] Substituting the ideal gas equation of state $p = n_g k_B T_g$ and the mean free path of electron-neutral collision $\lambda = 1/(\sigma_{en} n_g)$, with n_g being the neutral gas density, into Eq. (1), we obtain a linear relationship between the most effective discharge path and the electron mean free path

$$d_{\text{Stoletov}} = C\lambda, \tag{2}$$

where the ratio C is expressed as $C = \exp(1) \cdot \ln(1/\gamma)$. Equation (2) tells that to obtain the lowest breakdown voltage U_{min}, the discharge tends to automatically optimize its path, whose length is determined by the electron mean free path. As shown in Fig. 3, as the pressure decreases, the electron mean free path increases, so does the effective discharge path length. Similar phenomena of the discharge path versus gas pressure are experimentally observed in Ref. 15.

For the combined Paschen's curve in Fig. 2, in the right branch (at high pressure), the discharge tends to occur across the shortest gap distance d_{min}, and the breakdown curve is close to that in the 50–μm parallel-plate gap. In the left branch (at low pressure), the discharge tends to occur across the longest gap distance d_{max}, and the breakdown behavior is similar to that in the 500–μm parallel-plate gap. Between the two minimums (see Fig. 2), the discharge automatically optimizes its discharge path, which results in a flattened Paschen's curve having relatively low breakdown voltages close to U_{min} in a wide pressure range. The effects of the protrusion height a and the protrusion radius b, as well as the discharge polarity, on the Paschen's curve will be presented as follows.

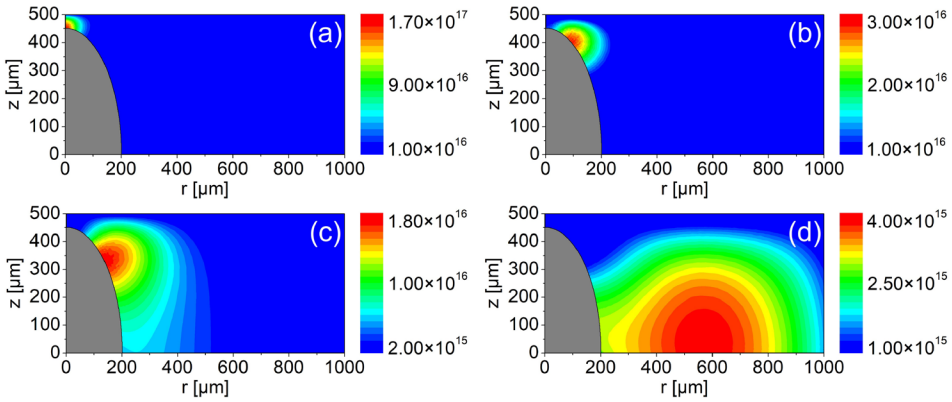

FIG. 3. The discharge channel represented by ion densities (m^{-3}) in the microgap with a cathode surface protrusion at different pressures, (a) 500 Torr, (b) 100 Torr, (c) 50 Torr, and (d) 10 Torr. In the simulations, $U_{dc} = 150$ V.

The effect of the protrusion radius is shown in Fig. 4(a), and the effect of the discharge polarity is shown in Figs. 4(b)–4(d). The protrusion height a is fixed at 450 μm, and the protrusion radius b ranges from 200 to 600 μm. It can be seen in Fig. 4(a) that the difference of Paschen's curves caused by changing the protrusion radius is recognized in the left branch but less obvious in the right branch. In the high-pressure regime, since the protrusion height a and the d_{min} are fixed, the discharge occurs along the shortest path, not affected by the increase in the protrusion radius. Thus, the Paschen's curves overlap in the right branch. In the low-pressure regime, the discharge has a longer path and the ion-impact secondary emission mainly occurs on the cathode substrate, see Fig. 3(d). When the protrusion radius is larger, the effective cathode substrate area for the ion-impact flux becomes smaller, which needs a higher voltage to ignite the discharge. Thus, in the left branch, the smaller the protrusion radius, the lower the breakdown curve.

In Figs. 4(b)–4(d), the effect of discharge polarity on the Paschen's curve seems minor. However, it still shows a tendency that with an anode protrusion, it has a slightly lower breakdown voltage in the left branch of Paschen's curve but a slightly higher breakdown voltage in the right branch. Similarly, this can be explained by the effective ion-impact flux on the cathode surface. At low pressures, the cathode effective emission area with an anode protrusion is larger than that with a cathode protrusion. Also, with an anode protrusion, the diverging (with respect to the center of the cathode) field lines (see Fig. 6 below) result in a higher ion flux toward the effective emission area of the flat cathode, whereas with a cathode protrusion, the diverging field lines towards the center lead to a lower ion flux toward the effective emission area of the flat cathode substrate. The combination of these two factors results in a lower breakdown voltage in the left branch for the anode protrusion cases. As shown in Figs. 4(b)–4(d), the smaller the area of the flat cathode substrate, the larger the difference in the left branch caused by the discharge polarity. At high pressures, the discharge occurs between the protrusion tip and the opposite electrode. In this situation, the field enhancement should be considered. With a cathode protrusion, the electric field is enhanced near the cathode tip, and consequently, the cathode

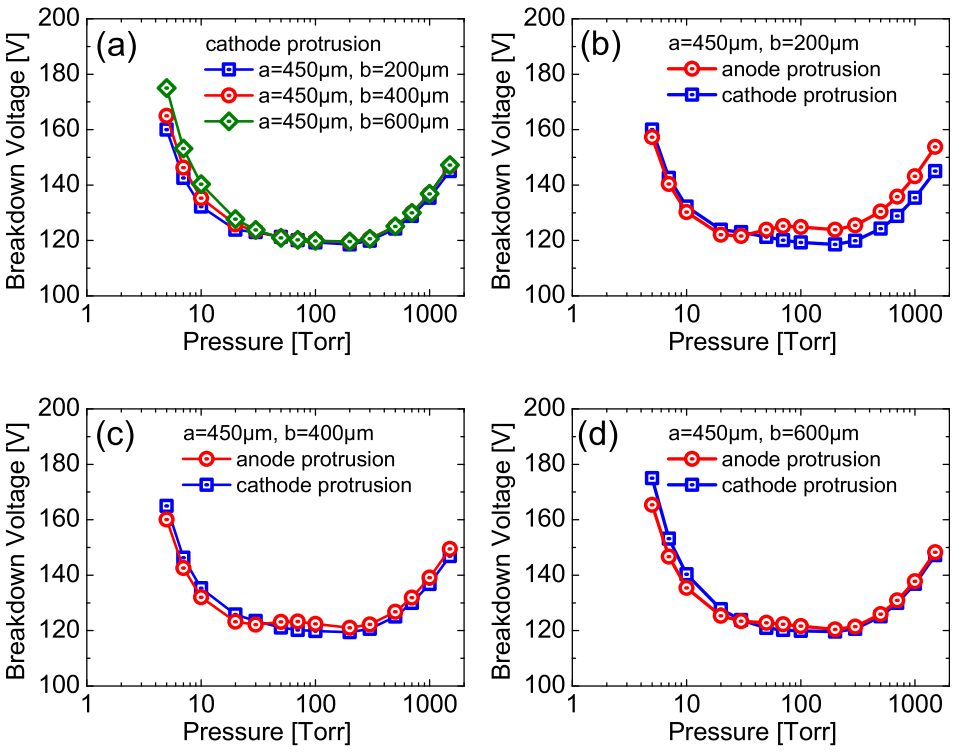

FIG. 4. (a) Paschen's curve in a microgap with a cathode protrusion having the same height but different radii and (b)–(d) comparison of the discharge polarity on Paschen's curve with different protrusion radii.

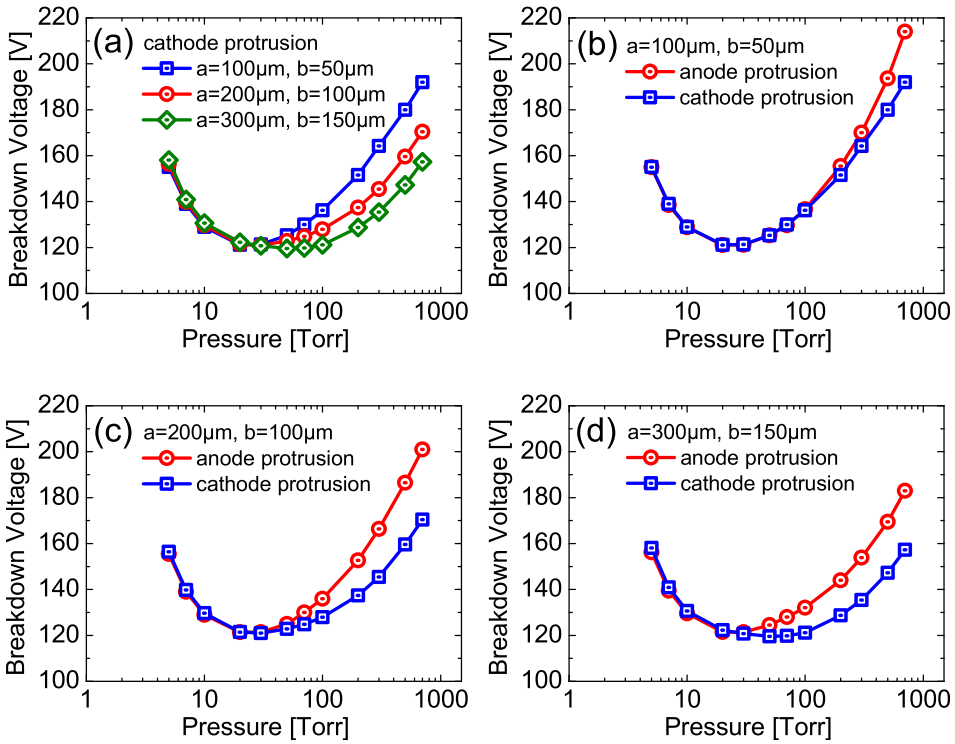

FIG. 5. (a) Paschen's curve in the microgap with a cathode protrusion having the same aspect ratio but different heights; (b)–(d) the effect of the discharge polarity on Paschen's curve.

ion-impact flux becomes more efficient, whereas with an anode protrusion, the electric field is more enhanced near the anode with less space charge effect in the Townsend regime and then the cathode ion-impact flux is less efficient. Also note that at high pressures the discharge is contracted in the centre, and the electric field lines (see Fig. 6 below) towards the cathode center are converging with a cathode protrusion while diverging with an anode protrusion. Therefore, the breakdown voltage with a cathode protrusion is lower than that with an anode protrusion in the right branch. Since the field enhancements generally are not severe (within one order) here, the difference between the Paschen's curves caused by the discharge polarity is not large. The field enhancement decreases as the protrusion radius becomes larger and the polarity effect in the right branch gradually disappears, as shown in Figs. 4(b)–4(d).

The effect of the protrusion height is shown in Fig. 5(a), and the effect of the discharge polarity is shown in Figs. 5(b)–5(d). In order to maintain roughly the same field enhancement while changing the protrusion height, the aspect ratio of the surface protrusion is fixed.[39] It can be seen in Fig. 5(a) that the impact of the protrusion height on the Paschen's curve is more distinguishable in the right branch and almost negligible in the left branch. This phenomenon can be explained in a similar way as before. The discharge at low pressure is determined by the longest gap distance $d_{\max}$ which is the same for the cases in Fig. 5(a). The discharge at high pressure is determined by the shortest gap distance $d_{\min}$ which decreases as the protrusion height a increases. At a specific pressure in the right branch, the higher the protrusion, the smaller the $d_{\min}$ and then the lower the breakdown voltage. The effect of the discharge polarity in Figs. 5(b)–5(d) is clearly observed in the right branch of the Paschen's curve. As is mentioned before, this is due to different electric field enhancements caused by the protrusion on the anode or the cathode. A larger field enhancement near the cathode protrusion tip results in lower breakdown voltages than that with an anode protrusion.

The impacts of the anode and the cathode protrusion on discharge processes are illustrated in Fig. 6. For the given microgaps with different polarities, the key parameters are the shortest gap distances ($d_{\min1}$ and $d_{\min2}$), the longest gap distances ($d_{\max1}$ and $d_{\max2}$), the electric field enhancement between the protrusion tip and the opposite electrode (E_{en1} and E_{en2}), and the effective cathode emission areas (S_{flux1}

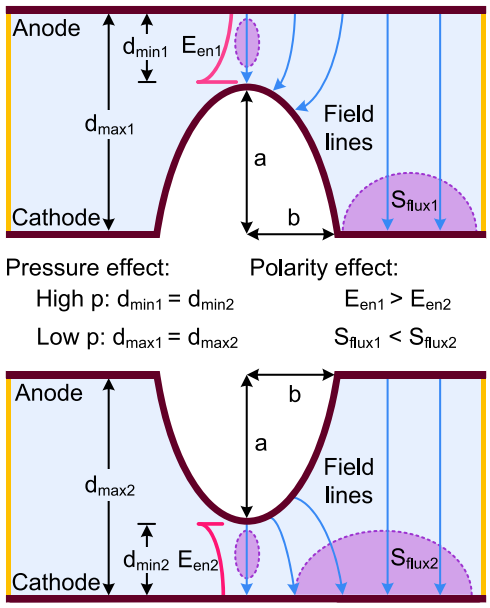

FIG. 6. Illustration of the impacts of anode and cathode protrusions on discharge processes. $d_{\min1}$ and $d_{\min2}$ are the shortest discharge paths at high pressure; E_{en1} and E_{en2} represent the electric field enhancement between the protrusion tip and the opposite electrode at high pressure; $d_{\max1}$ and $d_{\max2}$ are the longest discharge paths at low pressure; S_{flux1} and S_{flux2} are the effective cathode emission areas at low pressure.

and S_{flux2}). d_{max} is directly determined by the parallel-plate microgap, while d_{min}, S_{flux}, and E_{en} are closely related to the protrusion height a, radius b, and aspect ratio a/b, respectively. Whether d_{max} and d_{min} come into play depends on the gas pressure or more exactly the electron mean free path. For the discharge polarity effect, the difference of the field enhancement E_{en} at high pressure and the effective cathode emission area S_{flux} at low pressure should be considered to determine where the discharge occurs. Generally, by changing only the polarity for a given gap, i.e., when $d_{min1} = d_{min2}$ and $d_{max1} = d_{max2}$, the larger E_{en} and S_{flux} can both result in lower breakdown voltages.

In summary, Paschen's curve in microgaps with a hemi-ellipsoidal electrode surface protrusion was quantified as the gas pressure varies from low to high pressure regimes, in which the discharges are dominated by the secondary electron emission and the field emission does not contribute. The surface protrusion on the cathode electrode results in a combined Paschen's curve, which transits from the long-gap behavior at low pressure to the short-gap behavior at high pressure, resulting in relatively low breakdown voltages in a wider pressure range. As the gas pressure transits from the low to the high pressure regime, the discharge automatically optimizes its discharge path to obtain the lowest breakdown voltage. At high pressure, the discharge occurring between the protrusion tip and the opposite electrode is mainly determined by the shortest gap distance as well as the electric field enhancement. At low pressure, the discharge occurring between the protrusion substrate and the opposite electrode is mainly characterized by the longest gap distance as well as the effective cathode emission area. This study elucidates key parameters for gas breakdown in microgaps with a surface protrusion over a wide range of pressures, which might be strategic to the design of microgaps with controlled breakdown voltage across many orders in pressure via the shaping of protrusions. Future work includes the effects of the shape of the surface irregularity and surface roughness on Paschen's curve. Since the majority of the studies on this topic are based on simulations, the corresponding experimental works are highly suggested.

This work was supported by the Air Force Office of Scientific Research (AFOSR) Grant No. FA9550-18-1-0062, the DOE Plasma Science Center Grant No. DE-SC0001939, and an MSU Strategic Partnership Grant. Peng Zhang was also supported by AFOSR YIP Award No. FA9550-18-1-0061.

[1]J. P. Boeuf, L. C. Pitchford, and K. H. Schoenbach, Appl. Phys. Lett. **86**, 071501 (2005).
[2]X. Tan and D. B. Go, J. Appl. Phys. **123**, 063303 (2018).
[3]A. M. Loveless and A. L. Garner, Appl. Phys. Lett. **108**, 234103 (2016).
[4]F. Paschen, Ann. Phys. **273**, 69 (1889).
[5]T. Shao, G. Sun, P. Yan, and S. Zhang, Jpn. J. Appl. Phys., Part 1 **46**, 803 (2007).
[6]Y. Fu, Y. Shuo, X. Zou, H. Luo, and X. Wang, Phys. Plasmas **23**, 093509 (2016).
[7]J. T. Gudmundsson and A. Hecimovic, Plasma Sources Sci. Technol. **26**, 123001 (2017).
[8]Y. Fu, Y. Shuo, X. Zou, H. Luo, and X. Wang, Phys. Plasmas **24**, 023508 (2017).
[9]N. Bhattacharjee, A. Urrios, S. Kang, and A. Folch, Lab Chip **16**, 1720 (2016).
[10]S. Martínez-Jarquín, A. Moreno-Pedraza, H. Guillén-Alonso, and R. Winkler, Anal. Chem. **88**, 6976 (2016).
[11]J. A. Buendia and A. Venkattraman, Europhys. Lett. **112**, 55002 (2015).
[12]Y. Fu, P. Zhang, J. P. Verboncoeur, A. J. Christlieb, and X. Wang, Phys. Plasmas **25**, 013530 (2018).
[13]Y. Fu, P. Zhang, and J. P. Verboncoeur, Appl. Phys. Lett. **112**, 254102 (2018).
[14]Z. L. Petrović, N. Škoro, D. Marić, C. M. O. Mahony, P. D. Maguire, M. Radmilović-Rađenović, and G. Malović, J. Phys. D: Appl. Phys. **41**, 194002 (2008).
[15]D. Marić, N. Škoro, P. D. Maguire, C. M. O. Mahony, G. Malović, and Z. L. Petrović, Plasma Sources Sci. Technol. **21**, 035016 (2012).
[16]D. Levko and L. L. Raja, J. Appl. Phys. **117**, 173303 (2015).
[17]A. Venkattraman, A. Garg, D. Peroulis, and A. A. Alexeenko, Appl. Phys. Lett. **100**, 083503 (2012).
[18]D. B. Go and A. Venkattraman, J. Phys. D: Appl. Phys. **47**, 503001 (2014).
[19]M. Radmilović-Radjenović, Š. Matejčik, M. Klas, and B. Radjenović, J. Phys. D: Appl. Phys. **46**, 015302 (2013).
[20]J. S. Townsend, *Electricity in Gases* (Clarendon Press, Oxford, 1915).
[21]Y. P. Raizer, *Gas Discharge Physics* (Springer, Berlin, 1991).
[22]D. Levko and L. L. Raja, Phys. Plasmas **23**, 073513 (2016).
[23]M. Radmilović-Radjenović and B. Radjenović, Plasma Sources Sci. Technol. **17**, 024005 (2008).
[24]D. B. Go and D. A. Pohlman, J. Appl. Phys. **107**, 103303 (2010).
[25]R. Tirumala and D. B. Go, Appl. Phys. Lett. **97**, 151502 (2010).
[26]A. Semnani, A. Venkattraman, A. A. Alexeenko, and D. Peroulis, Appl. Phys. Lett. **102**, 174102 (2013).
[27]A. Peschot, N. Bonifaci, O. Lesaint, C. Valadares, and C. Poulain, Appl. Phys. Lett. **105**, 123109 (2014).
[28]A. M. Loveless and A. L. Garner, Phys. Plasmas **24**, 113522 (2017).
[29]A. Derzsi, I. Korolov, E. Schüngel, Z. Donkó, and J. Schulze, Plasma Sources Sci. Technol. **24**, 034002 (2015).
[30]A. V. Phelps and Z. L. Petrović, Plasma Sources Sci. Technol. **8**, R21 (1999).
[31]G. J. M. Hagelaar and L. C. Pitchford, Plasma Sources Sci. Technol. **14**, 722 (2005).
[32]T. Farouk, B. Farouk1, D. Staack, A. Gutsol, and A. Fridman, Plasma Sources Sci. Technol. **15**, 676 (2006).
[33]Y. Fu, H. Luo, X. Zou, and X. Wang, Plasma Sources Sci. Technol. **23**, 065035 (2014).
[34]Y. Fu, J. P. Verboncoeur, and A. J. Christlieb, Phys. Plasmas **24**, 103514 (2017).
[35]V. A. Lisovskiy, S. D. Yakovin, and V. D. Yegorenkov, J. Phys. D: Appl. Phys. **33**, 2722 (2000).
[36]V. A. Lisovskiy, R. O. Osmayev, A. V. Gapon, S. V. Dudin, I. S. Lesnik, and V. D. Yegorenkov, Vacuum **145**, 19 (2017).
[37]R. R. Arslanbekov and V. I. Kolobov, J. Phys. D: Appl. Phys. **36**, 2986 (2003).
[38]L. Xu, A. V. Khrabrov, I. D. Kaganovich, and T. J. Sommerer, Phys. Plasmas **24**, 093511 (2017).
[39]J. Lin, P. Y. Wong, P. Yang, Y. Y. Lau, W. Tang, and P. Zhang, J. Appl. Phys. **121**, 244301 (2017).